The effect of entrainment through atmospheric boundary layer growth on observed and modeled surface ozone in the Colorado Front Range

L. Kaser[1] [ID], E. G. Patton[1] [ID], G. G. Pfister[1] [ID], A. J. Weinheimer[1] [ID], D. D. Montzka[1] [ID], F. Flocke[1] [ID], A. M. Thompson[2] [ID], R. M. Stauffer[2,3] [ID], and H. S. Halliday[4,5]

[1]National Center for Atmospheric Research, Boulder, Colorado, USA, [2]NASA Goddard Space Flight Center, Greenbelt, Maryland, USA, [3]Universities Space Research Association, Columbia, Maryland, USA, [4]Department of Meteorology and Atmospheric Science, Pennsylvania State University, University Park, Pennsylvania, USA, [5]Now at NASA Langley Research Center, Hampton, Virginia, USA

Abstract Ozone concentrations at the Earth's surface are controlled by meteorological and chemical processes and are a function of advection, entrainment, deposition, and net chemical production/loss. The relative contributions of these processes vary in time and space. Understanding the relative importance of these processes controlling surface ozone concentrations is an essential component for designing effective regulatory strategies. Here we focus on the diurnal cycle of entrainment through atmospheric boundary layer (ABL) growth in the Colorado Front Range. Aircraft soundings and surface observations collected in July/August 2014 during the DISCOVER-AQ/FRAPPÉ (Deriving Information on Surface conditions from Column and Vertically Resolved Observations Relevant to Air Quality/Front Range Air Pollution and Photochemistry Éxperiment) campaigns and equivalent data simulated by a regional chemical transport model are analyzed. Entrainment through ABL growth is most important in the early morning, fumigating the surface at a rate of ~5 ppbv/h. The fumigation effect weakens near noon and changes sign to become a small dilution effect in the afternoon on the order of −1 ppbv/h. The chemical transport model WRF-Chem (Weather Research and Forecasting Model with chemistry) underestimates ozone at all altitudes during this study on the order of 10–15 ppbv. The entrainment through ABL growth is overestimated by the model in the order of 0.6–0.8 ppbv/h. This results from differences in boundary layer growth in the morning and ozone concentration jump across the ABL top in the afternoon. This implicates stronger modeled fumigation in the morning and weaker modeled dilution after 11:00 LT.

1. Introduction

Elevated tropospheric ozone levels can result in respiratory and cardiorespiratory diseases and increased mortality from both short-term and long-term exposure [*World Health Organization*, 2013]. A recent study by *Fann et al.* [2012] found that 4700 deaths in the U.S. were related to tropospheric ozone in 2005. In the Denver Metro area, an average of 45 days a year (based on data from 2006 to 2015) reached values classified on the air quality index as "unhealthy for sensitive groups" or above ("unhealthy" and "very unhealthy") [*AirNow, A look back: Ozone in*, 2015]. Several counties in the Colorado Front Range, encompassing the cities of Denver, Boulder, Greeley, Ft. Collins, and Loveland, were recently classified as being in a moderate nonattainment area with respect to ozone [*Environmental Protection Agency*, 2016]. In addition to impacts on human health, elevated ozone concentrations damage plants and lead to a 3–12% decrease in yields depending on crop type [*van Dingenen et al.*, 2009].

Ozone concentrations in the Earth's atmospheric boundary layer (ABL) are controlled by the balance between net chemical production, advection, entrainment, and deposition. The sum of these processes therefore influences the net variation of ozone concentrations at the surface. Each of these individual processes can vary in strength and by location throughout the day. To design effective regulatory strategies for ozone, the local ozone budget needs to be understood.

Tropospheric ozone is produced as a secondary pollutant due to atmospheric oxidation of carbon monoxide and hydrocarbons in the presence of NO_x [e.g., *Liu et al.*, 1992; *Chameides et al.*, 1992]. This process is driven by solar radiation and is therefore typically strongest during midday [e.g., *Cazorla et al.*, 2012; *Baier et al.*, 2015].

Ozone production is also strongly influenced by the availability of NO_x and hydrocarbons [*Kleinman*, 2005] both originating from a vast variety of natural and anthropogenic sources.

Once produced, tropospheric ozone can be transported over long distances due to its relatively long atmospheric lifetime [*Stevenson et al.*, 2006; *Jacob et al.*, 1999]. *Dentener et al.* [2011] report an ozone lifetime of hours to days in the ABL and a lifetime of weeks to months in the free troposphere. The lifetime of ABL ozone for this study is expected to be days because of the latitude and generally low humidity in Colorado.

The temperature inversion across the top of the boundary layer inhibits air exchange between the ABL and the overlying free troposphere, which can lead to an ozone concentration gradient between the atmospheric boundary layer and the air above [e.g., *Denmead et al.*, 1996]. Especially during the night, this inversion can lead to lower ozone concentrations in the ABL than above, because ozone in the ABL can both be deposited [*Wesely and Hicks*, 2000] and titrated by reaction with NO [*Logan et al.*, 1981]. In contrast, ozone in the residual layer (RL) and free troposphere (FT) has a much longer lifetime as there is no contact with the surface, and therefore no deposition, as well as much smaller NO_x concentrations decreasing both titration and permanent loss through formation of NO_3 and N_2O_5. During the daytime, as the ABL grows, both RL and FT air can be entrained into the ABL. The ozone concentration in the RL is determined by the surface concentrations of the previous night at the time the ABL collapses. The FT typically experiences larger wind speeds and is associated with long-range transport of ozone. Depending on the overlying concentrations relative to ABL concentrations, the ABL growth will either lead to a fumigation effect or a diluting effect. Long-range transported ozone pollution in the FT and residual ozone in the RL can therefore lead to a direct polluting effect on surface ozone or an inhibited dilution effect.

Both *Parrish et al.* [2010] and *Jaffe* [2011] found strong influences of free tropospheric air on surface ozone concentrations in California and in the Western U.S. on multiannual data sets indicating the importance of entrainment on surface air quality. A multiyear study by *Jaffe* [2011] found the highest correlations between surface ozone and free tropospheric ozone in the Western U.S. during July for monthly values and during August for daily values. July and August are therefore expected to be best suited to study this correlation in further detail as interaction between surface and free troposphere is strongest.

Combining all the processes of photochemical production and loss, advection, entrainment, and deposition creates a diurnal evolution of ozone in the ABL. *Lenschow et al.* [1981] used this budget approach, measuring all meteorological terms, including an ozone deposition velocity of 0.47 cm/s, to infer chemical ozone production rates. During their 19 September 1979 case study, they report an ozone production rate of 5.1 ppbv/h (2.42 ng m^{-3} s^{-1}) between 10:00 and 12:00 LT over the Colorado Front Range. During DISCOVER-AQ/FRAPPÉ (Deriving Information on Surface conditions from Column and Vertically Resolved Observations Relevant to Air Quality/Front Range Air Pollution and Photochemistry Éxperiment), *Baier et al.* [2017] report a measured median ozone production in Golden, CO of 5–10 ppbv/h between 10:00 and 12:00 LT. Many investigators have followed the strategy of *Lenschow et al.* [1981] to measure all but one term in the budget and infer the residual budget term [e.g., *Conley et al.*, 2011; *Trousdell et al.*, 2016]. *Kleinman et al.* [1994] calculated entrainment based on the difference between the ozone change expected due to calculated photochemical production and the observed ozone change. *Baier et al.* [2015] directly measured net ozone production, estimated entrainment to be small, and inferred advection terms necessary to close the budget. Most recently, *Trousdell et al.* [2016] investigated seasonal variability in daytime entrainment velocity in California and inferred differences in ozone production as a residual from the budget.

In this study we focus on understanding the diurnal cycle of ozone entrainment through ABL growth in the Colorado Front Range, using a zeroth-order jump model [*Tennekes*, 1973; *Fedorovich et al.*, 2004] applied to over 200 aircraft soundings and surface trace gas measurements collected during the July/August 2014 DISCOVER-AQ/FRAPPÉ. We analyze the ozone variability above and below the atmospheric boundary layer height (z_i), the evolution of ozone in both regions throughout the day, and the boundary layer growth rate. We evaluate model predictions from the Weather Research and Forcasting Model with Chemistry (WRF-Chem) against the observational results by interpolating model data in time and space to match the aircraft soundings.

WRF-Chem is widely used by the community trying to understand and predict air quality [e.g., *Fast et al.*, 2006; *Chuang et al.*, 2011; *Pfister et al.*, 2013; *Pagowski et al.*, 2010]. However, in regional-scale applications of WRF-Chem the physical processes of the atmospheric boundary layer are largely parameterized [*Hu et al.*, 2010]. Due to the aforementioned potential for long-range transport to impact local surface ozone

concentrations, it is therefore essential that the community understands any potential biases in WRF-Chem and their impact on surface ozone resulting from parameterizations of turbulent transport in the ABL.

Although model-observation comparisons of total ozone concentrations at various locations and altitudes have been conducted numerous times [e.g., *Pfister et al.*, 2013; *Im et al.*, 2015; *Mar et al.*, 2016], to the authors' knowledge, this is the first explicit evaluation of the average diurnal cycle of ozone entrainment through ABL growth between observations and a chemical transport model. Specifically, we separately compare influencing factors like absolute boundary layer height, boundary layer growth, and the ozone concentration jump across the top of the boundary layer. Diurnal cycles of entrainment through ABL growth from the observations and the model are compared to the total change in ozone over time to determine the influence of entrainment through ABL growth on surface ozone.

2. Data and Model

2.1. DISCOVER-AQ Colorado and FRAPPÉ Campaigns

In the summer of 2014 (15 July to 15 August), a large initiative focused on studying the air quality in the Colorado Front Range. Meteorological and chemical measurements on board three aircraft (NCAR C-130, NASA P-3B, and NASA B-200), as part of the DISCOVER-AQ and FRAPPÉ initiatives, were combined with numerous surface-based measurements of meteorological and chemical species at several sites in the Colorado Front Range. The flight patterns of all three aircraft and the full data set including data from surface sites are publicly available at http://www-air.larc.nasa.gov/missions/discover-aq/discover-aq.html [*DISCOVER-AQ Science Team,* 2016]. In this work we focus on evaluating model predictions of the effect of entrainment through ABL growth on daytime surface ozone in the Colorado Front Range. Figure 1 shows a map of the Colorado Front Range overlaid with a typical NASA P-3B flight track spiraling over six surface sites to collect in situ vertical information (section 2.2). Red circles indicate ozone surface measurements, magenta triangles indicate z_i measurements by a micropulse lidar (MPL), and green diamonds indicate z_i measurements by a ceilometer. The blue square represents a 3 km × 3 km box corresponding to the WRF-Chem model resolution.

2.2. Aircraft Data (NASA P-3B Soundings)

The NASA P-3B conducted consecutive soundings over Fort Collins (40.59°N, 105.11°W), Platteville (40.17°N, 104.76°W), Golden (39.77°N, 105.18°W), the Boulder Atmospheric Observatory (BAO) tower (40.06°N, 105.04°W), Denver-LaCasa (39.77°N, 104.97°W), and Chatfield Park (39.53°N, 105.03°W). This flight pattern was repeated 2–4 times a day, and the different sounding locations were connected together by low- (~1 km) or high- (5 km) altitude horizontal legs. During 24 flights on 16 flight days from 14 July to 10 August, a total of 214 aircraft soundings were collected ranging from 35 to 37 soundings per surface site. Flights typically occurred during fair weather conditions with low cloud coverage.

During the study period, sunrise occurred between 5:45 and 6:15 local time (LT), sunset between 20:28 and 19:45 LT, and solar noon was between 13:07 and 13:05 LT. To investigate the diurnal cycle of entrainment via ABL growth and its importance to surface ozone concentrations, all aircraft soundings were divided into four time periods: 7:00–9:00 LT, 9:00–11:00 LT, 11:00–13:00 LT, and 13:00–16:00 LT; this resulted in approximately 50–55 aircraft soundings per time bin. From the large number of meteorological and chemical variables measured onboard the NASA P-3B airplane, we primarily focus on ozone, NO_x, water mixing ratio, and potential temperature merged to 10 s averaged files. Ozone on the NASA P-3B was measured together with NO, NO_2, and NO_y by NCAR's four-channel chemiluminescence instrument [*Ridley and Grahek*, 1990; *Ridley et al.*, 1992]. The reported uncertainties are 0.1 ppbv +5%, 10 pptv +10%, and 20 pptv +10% for ozone, NO, and NO_2, respectively.

2.3. Surface Ozone and z_i Data

Surface ozone mixing ratios were measured at all six of the sites over which the NASA P-3B conducted soundings. At the BAO tower, ozone was measured close to the surface (6 m) and at 300 m above ground level (AGL) [*McClure-Begley et al.*, 2014]. The Colorado Department of Public Health and Environment (CDPHE) collected continuous surface ozone measurements at Golden, Chatfield, Denver, and Fort Collins. At the BAO tower at the surface and in Platteville, ozone measurements were conducted using a TECO 49c instrument and at the BAO tower at 300 m using a 2B Technologies sensor. Ozone concentration uncertainties reported
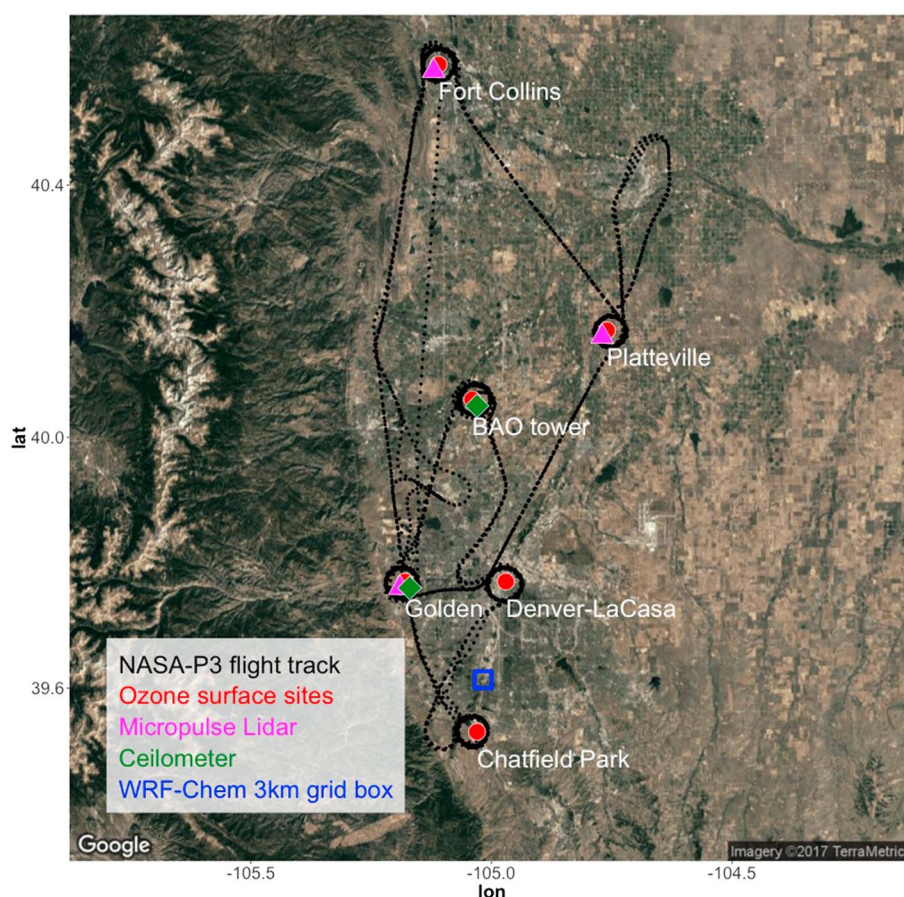
Figure 1. Map of the Colorado Front Range. The black dotted line indicates the typical flight pattern of the NASA P-3B. The white text close to the circles indicates name and location of the aircraft soundings. The red dots indicate the ozone surface site locations, magenta triangles the MPL measurements, and the green diamonds the ceilometer measurements. The blue box between Denver and Chatfield Park represents the size of a WRF-Chem 3 km grid box.

by CDPHE are ±4.6%, at the BAO tower ±1ppbv (± 1%), and in Platteville ±1.3%. All surface ozone data have been averaged to hourly mean values.

During the FRAPPÉ/DISCOVER-AQ campaign, two different instrument types measured the mixed layer height which we use here as a proxy for the atmospheric boundary layer depth (z_i). Ceilometers (Vaisala, CL51) [*Münkel*, 2007; *Schäfer et al.*, 2012] were deployed at the BAO tower and in Golden, and micropulse lidars (MPLs) [*Spinhirne*, 1993] were deployed at Fort Collins, Golden, and Platteville. The reported uncertainty of the MPLs and ceilometers is ±100 m and ±5 m, respectively.

2.4. WRF-Chem

This study uses the observations described in sections 2.2 and 2.3 to interrogate WRF-Chem simulations. We create virtual sounding profiles from the simulations by exporting model data at each grid point containing the NASA P-3B aircraft location determined using the aircraft's 10 s merge files. The profiles are then interpolated in the vertical to the aircraft altitude and directly compared to the observations. For the surface sites, model data are interpolated from instantaneous 10 min output to the time, location, and altitude of the surface observations. WRF-Chem version 3.6.1 [*Grell et al.*, 2005] is run using a two-domain configuration with the outer domain using a 15 km × 15 km resolution over the Western U.S. (94.15°W to 131.55°W and 28.63°N to 49.96°N) and the inner domain using a 3 km × 3 km resolution covering the state of Colorado (113.21°W to 100.99°W and 35.07°N to 42.36°N). Results from the inner domain are used here. We use 36 vertical levels from the surface to 10 hPa with 10 levels below 1 km. Level thicknesses range from 30 m for the lowest level to ~150 m at 1 km and 1000 m at 8 km above ground. Meteorological initial and boundary conditions are taken from the European Centre for Medium-Range Weather Forecasts (ECMWF) Interim

Reanalysis (ERA-Interim). Chemical initial and boundary conditions are taken from a Real-time Air Quality Modeling (RAQM) simulation [*Sullivan et al.*, 2015]. To avoid meteorological drift, WRF-Chem meteorological fields are weakly nudged and reinitialized every 24 h at 0 UTC with ERA-Interim analysis fields. The chemical fields are not nudged or reinitialized.

WRF-Chem was configured to use the Yonsei University (YSU) boundary layer scheme [*Hong et al.*, 2006; *Hong*, 2010], the Thompson microphysics scheme [*Thompson et al.*, 2008], the Rapid Radiative Transfer Model (RRTMG) radiation scheme [*Iacono et al.*, 2008], Grell 3-D ensemble cumulus scheme [*Grell*, 1993; *Grell and Devenyi*, 2002] for the outer domain and resolved convection for the inner domain, NOAH land surface model [*Chen and Dudhia*, 2001], and the Monin-Obukhov surface layer scheme [*Monin and Obukhov*, 1954; *Janjic*, 1996, 2002]. We employ WRF-Chem's MOZART chemical option coupled with the Model for Simulating Aerosol Interactions and Chemistry (MOSAIC) 4-binaerosol module. This scheme is described in more detail in *Knote et al.* [2014].

Anthropogenic emissions are from the EPA (Environmental Protection Agency) National Emission Inventory NEI 2011v2 but with mobile emissions reduced to 50%. This reduction is applied because a comparison between aircraft and surface observations over the Denver metro area reveal a high model bias in NO_x and is in line with an overestimation of the NEI 2011v2 NO_x mobile sector suggested by *Anderson et al.* [2014]. Biogenic emissions are calculated online using the Model of Emissions of Gases and Aerosols from Nature (MEGAN) [*Guenther et al.*, 2006], and fire emissions are taken from the Fire INventory from NCAR (FINN) [*Wiedinmyer et al.*, 2011]. A detailed namelist for the WRF-Chem simulation is given in Table S2 in the supporting information.

As will be shown also in this study, the evaluation with FRAPPÉ and DISCOVER-AQ measurements indicates an overall low bias of modeled free tropospheric ozone. One reason for this low model bias might be related to the model underrepresenting stratospheric-tropospheric exchange given that *Sullivan et al.* [2015] suggest an increase in ozone in the upper free troposphere between 10 and 30 ppbv during the period of the campaign with occasional influence on the lower free troposphere. Using the NEI 2011v2 for the 2014 time period is expected to lead to further uncertainties given the installation of various emission controls (e.g., reduced mobile emissions, conversion of the Cherokee power plant to natural gas) after 2011, while at the same time population and oil and gas activities in the NFRMA increased between 2011 and 2014. Lastly, boundary conditions and errors in ozone simulated in upwind regions might add to the overall low model bias. In this study, we investigate the impact of entrainment on this low bias.

2.5. HYSPLIT

The National Oceanic and Atmospheric Administration's (NOAA) Hybrid Single Particle Lagrangian Integrated Trajectory (HYSPLIT) Model [*Stein, et al.*, 2015; *Rolph*, 2016] is used to calculate back trajectories and to gain knowledge of air mass history. All trajectories are calculated using NARR (North American Regional Reanalysis) data with 35 km resolution, with a source location of Denver (39.75°N, 104.87°W) and a source height of 500 m AGL, all starting at 8:00 LT, but using wind fields for the actual days in July corresponding to the flight days of interest.

3. Methods

3.1. Determining z_i Using Aircraft Soundings

The ABL depth (z_i) for each NASA P-3B sounding is determined by locating the change in gradient or jump in concentration of potential temperature, relative humidity, ozone, and NO_x. At the top of the ABL the potential temperature gradient changes, and ozone, RH, and NO_x typically exhibit step changes because air exchange between the ABL and layers aloft is restricted. For some aircraft soundings this step change is very obvious (see supporting information, Figure S1a); other cases are less clear (Figure S1b). For the latter cases, the ABL depth measured by either the ceilometer or the micropulse lidar (MPL) is used if available. If no surface-based observations of z_i are available and tracer step changes from the aircraft soundings are ambiguous, the average z_i during that time of day is introduced to assist in determining z_i for that particular sounding. A detailed comparison of surface-based z_i measurements and z_i estimated from tracer step changes in the aircraft soundings for each measurement site is given in Figure S2. Figure S2 shows a good comparison

of surface-based z_i measurements from all available surface sites with estimations of z_i from the aircraft sounding data.

3.2. ΔO_3

The ozone concentration jump (ΔO_3) across the boundary layer top is calculated as the difference between the average concentration over the 300 m layer above and below z_i. A 300 m average is chosen because when binned into 2 h time intervals, the morning ABL grows at an average rate of 180 ± 20 m h^{-1} (discussed in section 4.2); with a growth rate of 180 ± 20 m h^{-1} air masses 320–400 m above z_i will be entrained into the ABL over a 2 h interval. Two hour intervals are chosen to ensure a sufficient number of aircraft soundings of approximately 50 per time window.

3.3. O_3 Entrainment Resulting From Diurnally Varying ABL Growth

Following *Lenschow et al.*'s [1981] definition, the mean ozone concentration budget in the boundary layer can be written as

$$\frac{\partial \overline{O_3}}{\partial t} = -\overline{u}_i \frac{\partial \overline{O_3}}{\partial x_i} - \frac{\partial \overline{O_3' w'}}{\partial z} + P_{\text{net}}(O_3) \tag{1}$$

This equation says that mean ozone concentration changes in the boundary layer are driven by mean advection, the vertical turbulent flux gradient. and net chemical production. Applying the mixed layer model [e.g., *Tennekes*, 1973; *Fedorovich et al.*, 2004], the vertical flux gradient can be approximated by the ozone flux at the top of the boundary layer (i.e., the entrainment flux) minus the ozone flux at the surface (deposition flux), divided by the ABL height (z_i). The vertical flux gradient then simplifies to

$$-\frac{\partial \overline{O_3' w'}}{\partial z} = -\left[\frac{-w_e \Delta O_3 - v_d O_3}{z_i} \right] = \frac{w_e \Delta O_3}{z_i} + \frac{v_d O_3}{z_i} \tag{2}$$

This describes the net effect of turbulent vertical transport of ozone on ozone concentrations in the mixed layer, where the first term describes the contribution from ozone entrainment and the second term from ozone deposition. The total boundary layer growth rate ($\frac{\partial z_i}{\partial t}$) results from a combination of 1) ABL turbulence actively entraining nonturbulent free-tropospheric air into the ABL and 2) large-scale vertical motion associated with large-scale convergence/divergence (w_S) [e.g., *Stull*, 1988]. Therefore, in a mixed-layer modeling framework, the turbulence-induced entrainment rate (or entrainment velocity, w_e) is expressed as

$$w_e = \frac{\partial z_i}{\partial t} - w_s \tag{3}$$

In (2), ΔO_3 is the ozone concentration jump across the ABL top (defined as above boundary layer ozone minus below boundary layer ozone). The growth rate of the boundary layer ($\frac{\partial z_i}{\partial t}$) is described in section 4.3, and an average overall available spatial locations is used to calculate the influence of entrainment as it varies through the day. Because the aircraft turning radius was too small, vertical wind velocity (w_S) measurements at the top of the ABL are not available for this study. Even though previous studies have shown that subsidence can influence ABL growth rates by a similar order of magnitude to turbulent entrainment and both can increase or decrease ABL growth rates [*Angevine*, 1999], we are only able to estimate the effect of subsidence using model results. In the WRF-Chem simulation, the average vertical wind velocity at z_i was -1.3 ± 1.0 cm/s. This model-predicted subsidence velocity suggests that we probably underestimate w_e by about 25% by only considering the boundary layer growth contribution (i..e., by representing the first term on the right hand side of (2) as $\left[\frac{\partial z_i}{\partial t} \Delta O_3 \right]/z_i$). We fully acknowledge this uncertainty in our analysis. We calculate this boundary layer growth-related entrainment consistently for both the observations and the model. For improved readability in the rest of the text, we use the term "entrainment effect through ABL growth" with full appreciation that boundary layer growth is only part of the picture. Figure 2 outlines the different terms of the entrainment through ABL growth that are compared between observations and model in this work.
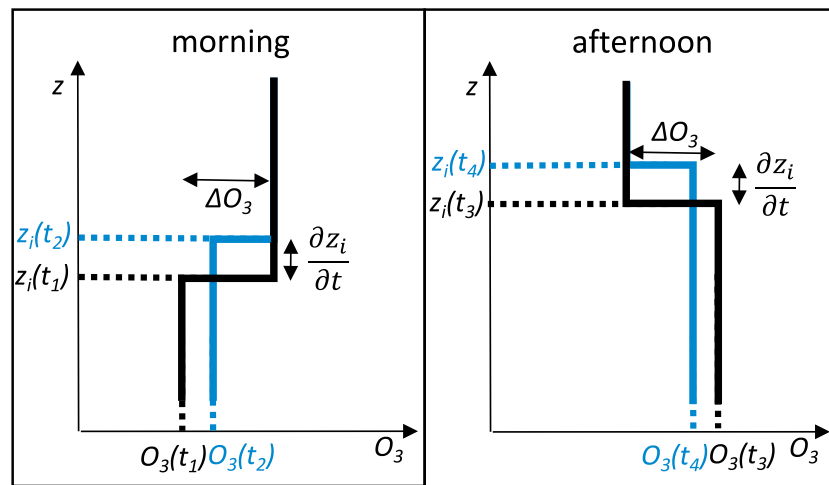
Figure 2. Schematic ozone profiles at varying times in an attempt to clarify how the observed and modeled ozone profiles are used to determine the magnitude of the first term on the right-hand side of equation (2). In the morning, ozone concentration above the ABL [$z > z_i(t_1)$] is larger than it is below $z_i(t_1)$ leading to a positive ΔO_3. Later in time (t_2), the boundary layer depth has increased from $z_i(t_1)$ to $z_i(t_2)$. This change in boundary layer height $\left(\frac{\partial z_i}{\partial t}\right)$ is used as our estimate of the entrainment velocity (w_e), because we have no subsidence velocity (w_s) measurements. As previously discussed, this could lead to an average error in estimating the true effect of entrainment of approximately 25% based upon the WRF-Chem's w_s prediction. Nevertheless, this boundary layer growth increases ozone concentrations in the boundary layer (blue profile), but the magnitude of the increase can be modulated by advection, deposition, and chemical production/loss. In the afternoon, ozone profiles in the ABL are typically quite different from those in the morning. ΔO_3 is negative and any boundary layer growth leads to a dilution of ozone in the boundary layer (blue trace at time t_4), with a similar caveat regarding the modulation of the ozone profiles by advection, deposition, and chemical production/loss. We investigate ΔO_3, z_i and $\frac{\partial z_i}{\partial t}$ derived from both the simulation and the observations to establish WRF-Chem's skill in predicting the influence of ABL growth on surface ozone concentrations. It is important to note that the schematic in Figure 2 presents a highly simplified picture since the ozone jump across the top of the boundary layer is not infinitely sharp nor are aircraft-observed ozone soundings perfectly smooth.

4. Results and Discussion

4.1. Ozone Aircraft Soundings and Their Diurnal Evolution

All 214 ozone soundings collected during the aircraft spirals over the Colorado Front Range sites are divided into four time windows (7:00–9:00 LT, 9:00–11:00 LT, 11:00–13:00 LT, and 13:00–16:00 LT). This partitioning leads to approximately 50 aircraft soundings per time window. Figures 3a–3d show all the ozone aircraft soundings for each of the time windows with each ozone aircraft sounding plotted as an individual blue line. The dark blue line represents the average sounding during each time window. The estimated ABL depth (see section 3.1) for each individual aircraft sounding is subtracted so that values on the negative y-axis indicate ozone concentrations within the ABL, and values on the positive y-axis are measured within the RL or FT. In both time windows before noon we observe slightly elevated ozone above the ABL in the average sounding, likely corresponding to ozone remaining from the previous day within the RL.

Because all the aircraft soundings begin/end at similar heights AGL, the increasing amount of data below zero between Figures 3a and 3d allow one to visualize the average increase in ABL depth between the different time windows. The ABL increases roughly from 400 m around 8:00 LT to 1000 m around 10:00 LT, to 1500 m around 12:00 LT, and to 2000 m around 14:30 LT (Section 4.3 presents a more detailed analysis of ABL growth throughout the day). Figures 3a–3d also reveal the large variability in ozone concentrations between different soundings—especially in the morning above the ABL, but visible throughout the day at all altitudes.

Figures 3e–3h show the WRF-Chem model predictions along the simulated flight track. Each individual aircraft sounding is plotted as a gray line and the average in black. The modeled ABL growth in this figure series is similar to the observations (see section 4.3 for more detail). Vertical ozone concentrations from the WRF-Chem simulations corresponding to the aircraft sounding locations (Figures 3e–3h show that sounding-to-sounding variability is well captured, though absolute ozone values predicted throughout the day and at
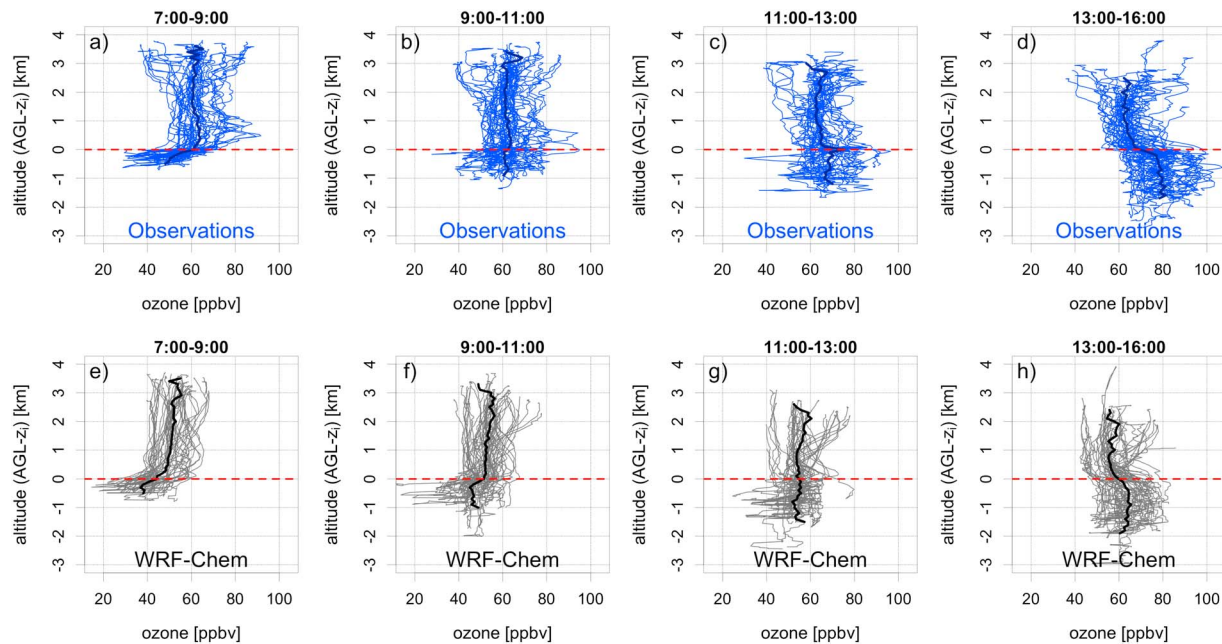
Figure 3. Ozone concentrations of all aircraft soundings (and all locations) between (a) 7:00–9:00 LT, (b) 9:00–11:00 LT, (c) 11:00–13:00 LT, and (d) 13:00–16:00 LT are plotted versus normalized altitude (AGL − z_i) so that all values below 0 km correspond to data within the ABL and all values above 0 km are concentrations observed above the ABL. The red dashed line indicates z_i. (e–h) The same for the WRF-Chem output along the flight tracks (Figures 3a–3d). The thicker dark blue and black lines in each plot show the average ozone sounding over all days for the observations and the model, respectively.

all altitudes are on the order of 10 ppbv lower than the observed concentrations. The vertical concentration variation in each sounding above the ABL is larger in the observations with an average standard deviation (std) of 5 ppbv than in the simulation with an average std of 3 ppbv. The reduced variance in the model likely results from both the model resolution and the overly dissipative nature of the numerical methods used to calculate advection.

The mean WRF-Chem vertical profile does not show the layer of elevated ozone above the ABL that is visible in the observations at 7:00–9:00 and 9:00–11:00.

4.2. Diurnal Cycle of Surface Ozone

Ozone concentrations are measured at the surface below all six aircraft sounding sites as well as additionally on the BAO tower at 300 m AGL. Average diurnal cycles of surface ozone during the flight days (17, 20–23, 27–29, 31 July and 2, 3, 6–8, 10 August) are shown in Figure 4. The average diurnal cycle on flight days over all six surface sites (black line) and the range of diurnal averages for the different sites (gray area) are compared to surface ozone from the WRF-Chem model (red). Broadly speaking, Figure 4 reveals decent agreement between the WRF-Chem simulation and the observations, as the shaded areas corresponding to the variability between the different sites mostly overlap. Average observed surface ozone concentrations (solid black line) increase by 6 ppbv/h from 8:00 to 14:00 LT. This increase is about 1 ppbv/h higher than predicted by WRF-Chem (solid red line), leading to an overall higher peak ozone concentration in the observations compared to the model; the modeled maximum also occurs 1 h later than in the observations. At nighttime and in the early morning (21:00–8:00 LT) the model is a few ppbv higher and throughout the day a few ppbv lower than the observations. Figures S3a–S3f analyze the surface sites individually. Diurnal cycles of surface ozone concentration compare differently at individual sites, but it should be noted that this comparison is between very localized measurements and model output from a simulation with 3 km spatial resolution. At most sites, modeled nighttime ozone is about 10 ppbv higher than the observations except for the Denver site where the modeled nighttime ozone is comparatively low and at the Golden site where nighttime ozone compares well. Throughout the day, simulated and observed surface ozone at Platteville and at the BAO tower agree best. In Golden, Denver, and Fort Collins modeled ozone increases about 1 h later and a weaker modeled growth leads to underprediction of the diurnal ozone maximum by 5–10 ppbv. In
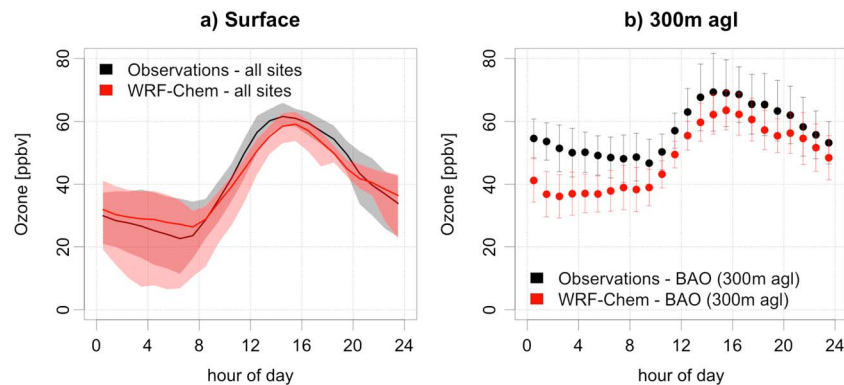
Figure 4. (a) The diurnal cycle during the flight days measured ozone averaged over all six surface sites in black, and the gray-shaded area shows the range of variation of the means for the different sites. In red, the same is shown for the WRF-Chem simulation. (b) The average diurnal cycle of ozone measured during the flight days at the BAO tower at 300 m above ground compared to model predictions at that same location and altitude.

Chatfield, modeled and observed ozone disagree mostly during the middle of the day (11:00–14:00 LT), with the model prediction being lower than the observations. Comparing the average over all sites between the observations and the model (Figure 4a) is a more robust and somewhat more appropriate comparison, since locally generated sampling biases in the observation are partly smoothed.

Modeled ozone concentrations corresponding to NASA P-3B locations are 10–15 ppbv lower than the observations at all altitudes and times (Figure 3). In contrast to this, averaged surface ozone concentration comparison between model and observations do not show this offset. To investigate this discrepancy, we introduce observations at 300 m on the tower at the BAO site (Figure 4b); similar to Figure 4a, the average diurnal cycle of observed ozone and its standard deviation (black) is compared to the model results from the grid point nearest to the site and altitude (red). Throughout the entire day (10:00 LT–20:00 LT) the model predicts 300 m ozone concentrations that are about 7 ppbv lower than observed. This difference is stronger in July with a low mean bias of 11 ppbv, whereas a lower bias (5 ppbv) is measured in August. The reasons for the low model biases are under investigation but are not the scope of this study. The modeled underprediction is strongest during the nighttime and early morning. During the daytime, observed ozone concentrations at BAO at the surface (Figure S3d) are on average ~5–15 ppbv lower than at 300 m (Figure 4b), indicating that ozone might not be well mixed within the ABL. The model, however, represents a more well-mixed ABL with similar ozone concentrations at the surface and at 300 m between 10:00 LT and 20:00 LT. Ozone lidar and sonde data similarly show a, in parts, high variability in ozone concentrations within the ABL, but also these are not well represented by the model (data not shown). *Zhang et al.* [2016] show in an analysis for DISCOVER-AQ over the Washington-Baltimore area in summer 2011 this vertical variability in NO_x aircraft soundings and its associated biases when modeling the boundary layer as well mixed.

4.3. Evolution of z_i Throughout the Day

Using the strategy outlined in section 3.1 to determine z_i, Figure 5 shows the average ABL height versus time during the flight days in summer 2014. Even though the complete diurnal cycle of z_i for the four surface sites with continuous z_i measurements is not linear at all times (Figure S4), the ABL height's variation during the time frame investigated by the aircraft soundings from 7:00 LT to 16:00 LT can be reasonably approximated as a linear function of time.

Different colors in Figure 5 indicate the different sounding locations. A linear fit through all the data (black line, Figure 5a) shows that z_i is observed to grow at a rate of 180 ± 20 m/h (5.0 ± 0.6 cm/s) on average. Linear fits to observed estimates of boundary layer depth evolution at each individual site are plotted in their respective colors; no site shows significantly different ABL growth compared to any other. Figure 5b shows a similar analysis for the virtual soundings through the WRF-Chem model space. Modeled boundary layer growth agrees well with the observations, with an average growth rate of 190 ± 20 m/h (5.3 ± 0.6 cm/s) on average. As in the observations, modeled ABL growth rates do not differ significantly by site.
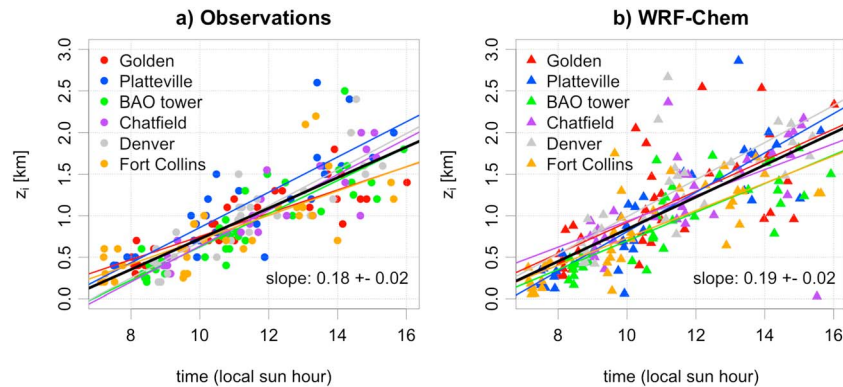
Figure 5. The ABL height for each aircraft sounding (determined according to the strategy outlined in section 3.1) and for all six surface sites (different colors) versus local time of day. Results (a) for the observations and (b) for WRF-Chem. The black line presents the average boundary layer growth estimated by a linear fit through all the available data. The colored lines present linear fits through all data from each individual site.

4.4. Diurnal Evolution of ΔO_3

To calculate the entrainment of ozone due to the growing boundary layer, one needs the absolute boundary layer height, the boundary layer growth rate, and the ozone jump across the top of the boundary layer (ΔO_3). The first two parameters have been discussed in sections 4.1 and 4.3. Here we analyze the diurnal evolution of ΔO_3 and connect the previously discussed ABL depth analysis with ΔO_3 to establish the diurnal evolution of ozone entrainment through ABL growth. The following data is from the aircraft soundings that do not include measurements at the surface, as the lowest NASA P-3B flight altitude was ~200 m AGL.

Figure 6 shows the distributions of mean ozone in the ABL (Figures 6a–6d), the distribution of mean ozone in the 300 m layer above the ABL (Figures 6e–6h), ΔO_3 (Figures 6i–6l), and the ozone entrainment through ABL growth (Figures 6m–6p) for the four time periods (7:00–9:00 LT, 9:00–11:00 LT, 11:00–13:00 LT, and 13:00–16:00 LT). The colors show the observations and the model results are plotted in black. The statistical results of the distributions (mean, minimum, and maximum) for observations, model, and difference of the two are summarized in Table 1. Ozone concentrations have a wide sounding-to-sounding variation on the order of 30–45 ppbv at all times both within and above the ABL. As this spread is relatively constant in time and altitude, and well captured by the model, we will subsequently consider only the mean values of the distribution to simplify the text.

Figures 6a–6d show that observed mean ozone concentrations in the ABL start in the morning (7:00–9:00 LT) at 52 ppbv and increase by 4–5 ppbv/h on average leading to an average ozone concentration of 79 ppbv in the afternoon. Boundary layer ozone in WRF-Chem also increases by 4–5 ppbv/h on average and agrees well with the observations from that perspective. However, the absolute values are 15 ppbv lower in the model than the observations. Similarly, Figures 6e–6h show the evolution of ozone in the first 300 m above the ABL, starting at an average of 61 ppbv for the observations, increasing at a rate of about 1–1.5 ppbv/h, and reaching an average of 68 ppbv in the afternoon. The model results start on average 15 ppbv lower in the early morning between 7:00 and 9:00 LT and increase more rapidly than the observations, that is, by 1.5–3 ppbv/h, ending up at 58 ppbv in the afternoon, now only about 10 ppbv lower than the observations. It should be noted, that this increase could result from a combination of photochemical production, long-range transport, and the general increase of ozone with altitude as expected in the FT; therefore, this value should only be compared between model and observations and not with other Eulerian time derivatives discussed in this section.

Figures 6i–6l combine ozone in the boundary layer and ozone 300 m above the boundary layer showing a mean observed ΔO_3 of 9 ppbv in the morning (7:00–9:00 LT), which matches that from the model, as the absolute 15 ppbv difference cancels out due to the subtraction. Observed ΔO_3 in the morning (7:00–9:00 LT) is in all but two out of the 37 aircraft soundings positive. The two outliers occurred on days (21 and 23 July) when especially clean free tropospheric air was transported into the Colorado area. Observed ΔO_3 decreases by 3 ppbv/h reaching −11 ppbv in the afternoon. Modeled ΔO_3 decreases slower with time (at
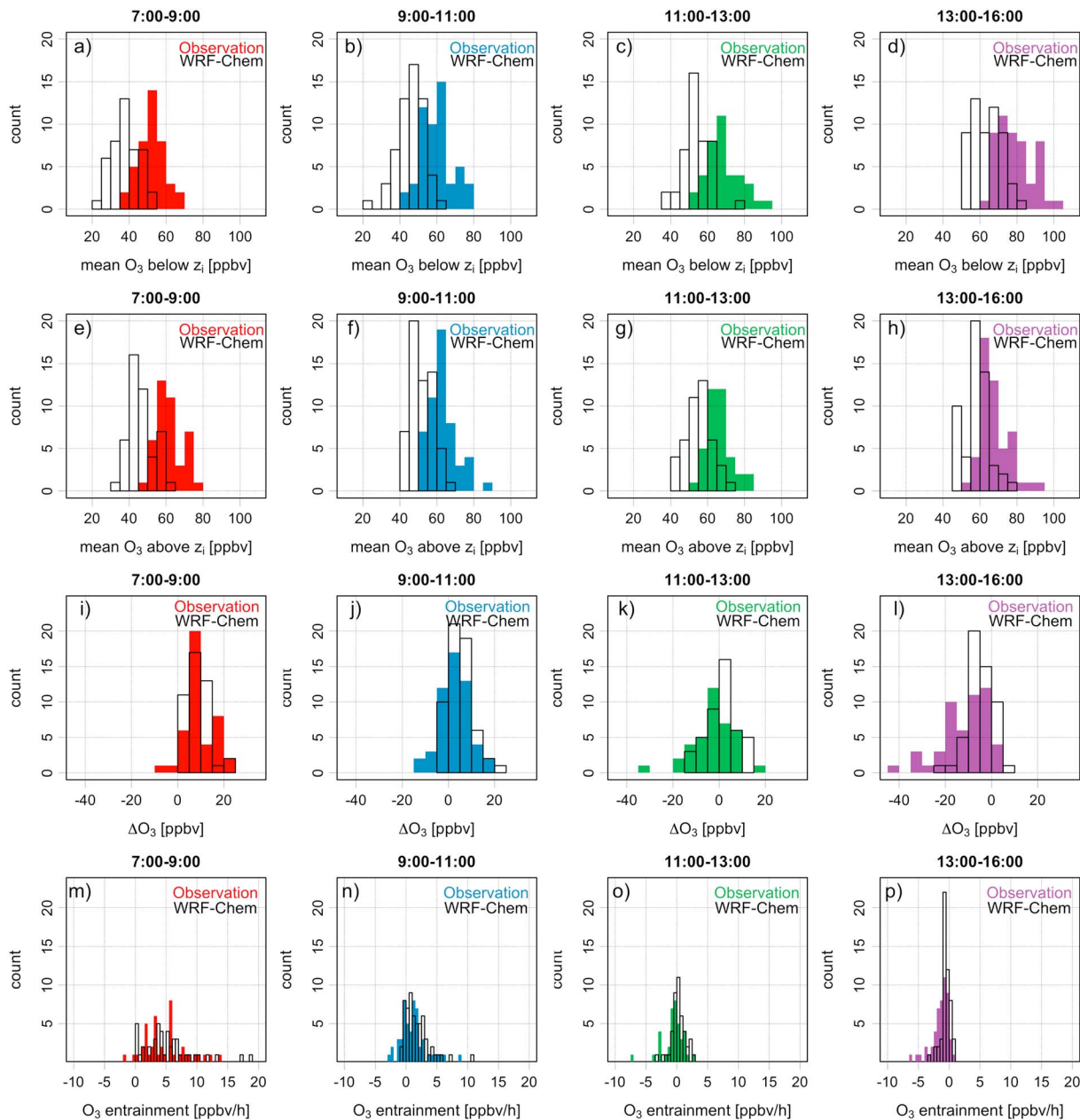
Figure 6. (a–d) The diurnal evolution of boundary layer ozone derived from the aircraft soundings in color for the observations and in black for the WRF-Chem model. (e–h) The diurnal evolution of ozone averaged over the first 300 m above the ABL. (i–l) Combination of the first two rows to show the diurnal evolution of ΔO_3 throughout the day. (m–p) The diurnal cycle of ozone entrainment through boundary layer growth $\left[\frac{\partial z_i}{\partial t} \, \Delta O_3\right]/z_i$, combining Figures 6i–6l with atmospheric boundary layer height and average boundary layer growth.

a rate of ~1.5–2.5 ppbv/h, reaching −5 ppbv in the afternoon) resulting from the fact that ozone above the ABL increases more strongly in the model than in the observations. This difference between observations and model is also reflected in the average time when ΔO_3 equals zero which was 11:00 LT in the observations and 12:00 LT in the model (Figure S5).

Finally—incorporating ABL growth, z_i and ΔO_3—Figures 6m–6p show the diurnal evolution of ozone entrainment through ABL growth (e.g., $\left[\frac{\partial z_i}{\partial t} \, \Delta O_3\right]/z_i$). If ΔO_3 is positive (increasing in z direction) and the boundary layer growing, ozone concentrations increase as a result. In this case, we define the contribution of ozone entrainment through ABL growth to the total ozone budget $\left[\frac{\partial z_i}{\partial t} \, \Delta O_3\right]/z_i$ as positive (note that the minus sign in (2) has been multiplied through). A growing boundary layer increases ozone concentrations in the

Table 1. Summary of Average, Minimum, and Maximum Values From the Distributions of Ozone Above the Boundary Layer, Below the Boundary Layer, ΔO_3, and Entrainment Through ABL Growth

Time Intervals:	7:00–9:00	9:00–11:00	11:00–13:00	13:00–16:00
Mean (min, max) ozone concentrations above z_i (ppbv)				
Observations:	51 (38, 66)	60 (43, 79)	69 (54, 90)	79 (63, 102)
WRF-Chem:	38 (24, 53)	46 (22, 63)	54 (39, 77)	64 (50, 82)
Difference:	14 (14, 13)	14 (21, 16)	15 (15, 13)	15 (13, 20)
Mean (min, max) ozone concentrations below z_i (ppbv)				
Observations:	61 (47, 76)	63 (52, 89)	66 (55, 85)	68 (54, 91)
WRF-Chem:	46 (32, 60)	52 (41, 67)	55 (42, 71)	58 (46, 78)
Difference:	15 (15, 16)	11 (11, 22)	11 (13, 14)	10 (8, 13)
Mean (min, max) ΔO_3 (O_3 above z_i – O_3 below z_i) (ppbv)				
Observations:	9 (22, −6)	3 (17, −12)	-3 (17, −33)	−11 (4, −40)
WRF-Chem:	9 (22, 1)	6 (24, −4)	1 (15, −11)	−5 (7, −21)
Difference:	0 (0, −7)	−3 (−7, −8)	−4 (2, −22)	−6 (−3, −19)
Mean (min, max) entrainment (ppbv/h)				
Observations:	4.8 (13.5, −1.7)	1.2 (8.6, −3.0)	−0.6 (2.7, −7.4)	−1.4 (0.6, −6.2)
WRF-Chem:	5.4 (18.6, 0.1)	1.8 (11.0, −0.8)	0.2 (2.9, −3.1)	−0.6 (0.8, −3.0)
Difference:	−0.6 (−5.1, −1.8)	−0.6 (−2.4, −2.2)	−0.8 (−0.2, −4.3)	−0.8 (−0.2, −3.2)

boundary layer for almost all morning soundings (between 7:00 and 9:00 LT) with an average increase of 4.8 ppbv/h. In the following hours, the mean ΔO_3 decreases, thereby decreasing entrainment's fumigation effect to 1.2 ppbv/h. On average, around 11:00 LT ΔO_3 changes sign, resulting in a small dilution effect of −0.6 ppbv/h to −1.4 ppbv/h. WRF-Chem captures the morning (7:00–9:00 LT) fumigation but tends toward a 0.6–0.8 ppbv/h stronger fumigation (or less dilution) than the observations throughout the rest of the day. The shift from fumigation to dilution (i.e., the change in sign of ΔO_3) occurs 1 h later in the model than in the observations. The difference in the morning values of entrainment through ABL growth is primarily influenced by the differences in the boundary layer growth rate (w_e) and absolute boundary layer height (z_i). After 11:00 LT, differences in model-predicted and observed entrainment through ABL growth result largely from ΔO_3 variations which increase throughout the day, because modeled boundary layer ozone does not increase as fast as observed boundary layer ozone. Accumulated over the course of the observed time from 7:00 LT to 16:00 LT, the difference in entrainment through ABL growth values between observations and model could lead to a modeled surface ozone of ~7 ppbv higher than found in the observations; this is not observed and therefore must be counteracted by other terms in the ozone budget such as chemical production/loss, deposition, horizontal, or vertical advection. The available data do not currently allow us to determine the exact process counteracting the entrainment through ABL growth difference in observations and model.

In a manner, similar to that which we have been discussing for ozone, we also investigated the entrainment through ABL growth of O_x ($O_3 + NO_2$) (Figure S7 and Table S1), finding that O_x in the boundary layer is 2–5 ppbv higher than O_3 in the boundary layer for the observations and 2–6 ppbv for the model. In the free troposphere, O_x and O_3 differ by 1 ppbv or less for the observations and 2 ppbv or less for the model. This difference results in an ΔO_x 2–3 ppbv smaller than ΔO_3 for the observations and 2–5 ppbv for the model. The largest difference between O_x and O_3 entrainment through ABL growth occurs in the morning, where that difference is 1.5 ppbv/h lower in the observations and 2.3 ppbv/h lower in the model. Later in the day the difference between O_x and O_3 entrainment through ABL growth reduces both for the observations and the model. Differences between observed and modeled O_x entrainment through ABL growth compared to that for O_3 are smaller in the morning and similar in the afternoon.

4.5. Origin of Different Ozone Concentrations Above the ABL

During FRAPPÉ/DISCOVER-AQ, background ozone concentrations are between 45 and 50 ppbv based on measurements along the western border of Colorado by the NCAR C-130, as well as on high-altitude surface stations (Longs Peak and Mines Peak) when winds are from the west. The lowest concentrations observed in the first 300 m above the boundary layer (Figures 6e–6h) are in this range but are highly variable with a spread of 35–45 ppbv. This day-to-day variability translates into a highly variable influence of ozone entrainment through ABL growth, especially in the morning where entrainment through ABL growth of ozone from
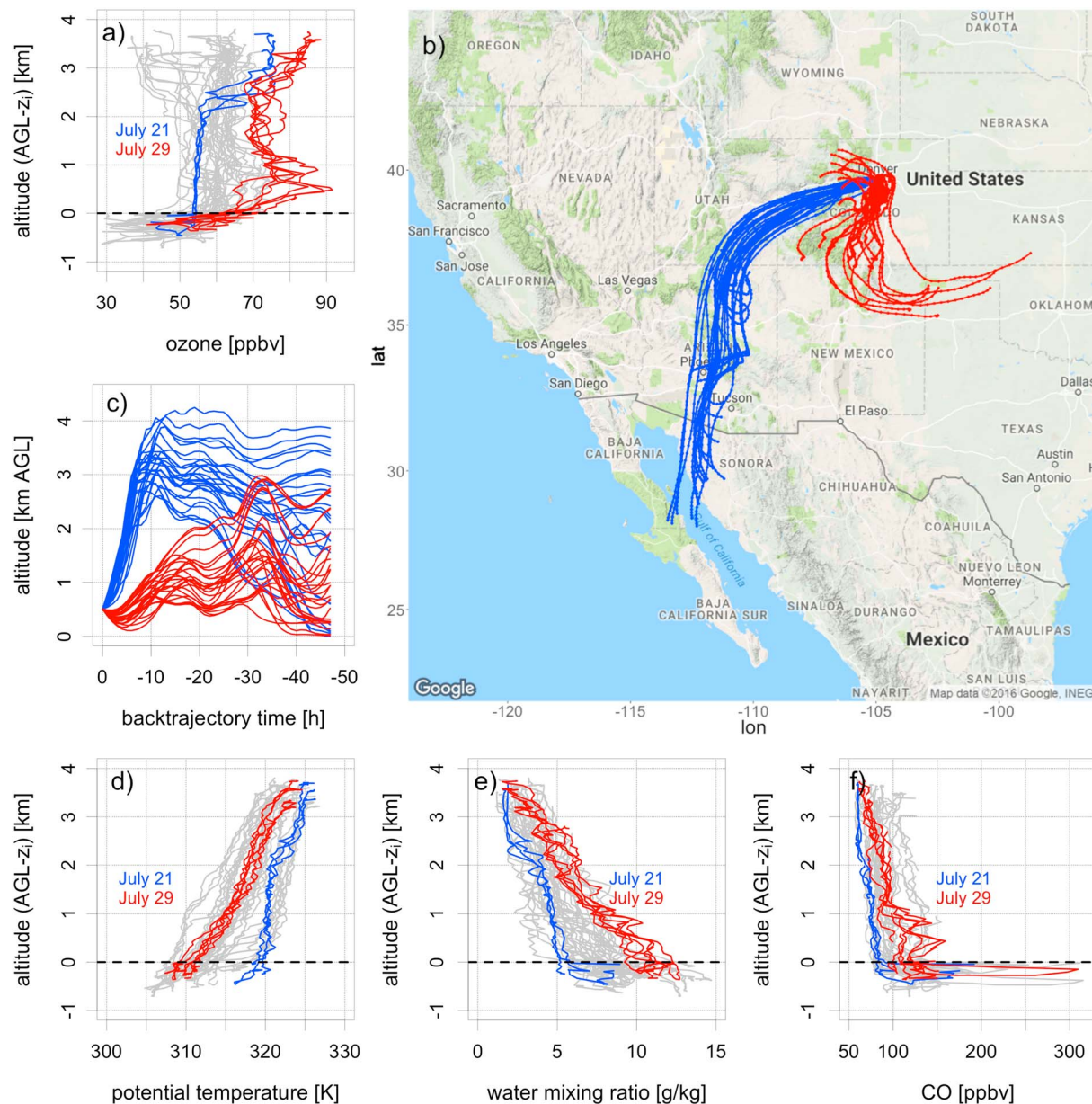
Figure 7. (a) Ozone concentrations from all soundings in the morning hours (7:00–9:00 LT) colored in gray; soundings for 21 July are overlaid in blue and for 29 July in red. The altitude is plotted as height AGL minus z_i of each individual sounding (as in Figure 3) so that values below 0 km are within the ABL and values above are above the ABL. (b and c) HYSPLIT back trajectories describing the origin of the 500 m air mass on 21 July (blue) and 29 July (red); horizontal back trajectory locations are plotted in Figure 7b and back trajectory altitude over time is plotted in Figure 7c. (d–f) The observed potential temperature, water mixing ratio, and carbon monoxide, respectively.

aloft is a dominant component controlling surface ozone concentrations. To offer insight into the mechanism driving this variability, we investigate the air mass history of the 2 days with the highest and lowest observed morning concentrations above the ABL (which could represent both RL or FT air). Figure 7a replots the data presented in Figure 3a with an emphasis on 21 July (blue, with one of the lowest ozone concentrations observed above the ABL during all the morning soundings) and 29 July (red, with the highest ozone concentrations observed above the ABL during all morning soundings). Ensemble HYSPLIT back trajectories are used to analyze the 500 m morning air masses of 21 and 29 July in the Denver area (Figures 7b and 7c, respectively). On 21 July, Figure 7a shows relatively low ozone concentrations above the boundary layer in the morning. The concentrations are also very uniform with altitude, ~55 ppbv in the first 2 km above the morning boundary layer. Back trajectories for the 48 h prior to 21 July show air
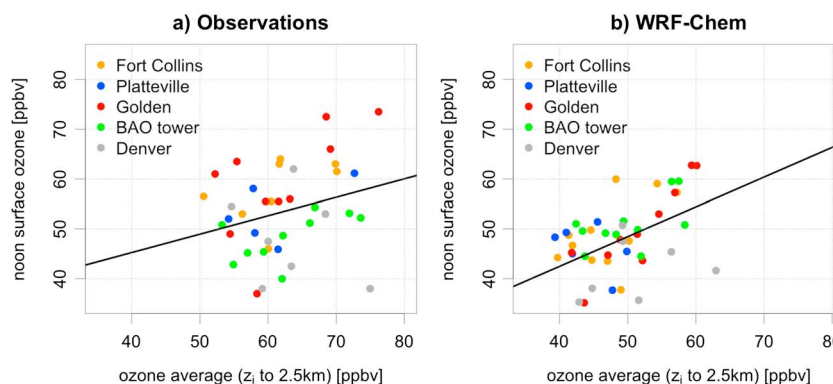
Figure 8. Noon time surface ozone concentrations versus morning (8:00 LT) ozone concentration averaged from the ABL up to 2.5 km are shown in color for each site, and the black line is the linear fit for all the data. Individual sites contain too little data to be statistically significant. Linear fits for 1 to 12 h of surface observations relative to the morning vertical average are shown in Table 2. The results for the linear fit at noon (4 h after the morning vertical average) are highlighted in bold. The analysis is conducted for both (a) the observations and (b) WRF-Chem.

masses transported over western continental North America high altitudes flowing over the mountains, and then downward into the Denver Metro Area. This is confirmed by relatively low water mixing ratio and high potential temperature and low CO concentrations measured in the aircraft soundings on 21 July (Figures 7d–7f). On 29 July, when we observe the highest morning ozone concentrations above the ABL, back trajectories indicate that the air mass sampled spent the previous 48 h at lower altitudes over Colorado and neighboring states. The 29 July air mass spent time in the ABL during the previous days and is therefore enhanced in terms of ozone concentrations, this is also visible in elevated water mixing ratio and elevated CO concentrations in the soundings collected in the morning hours (7:00–9:00 LT) above the ABL (Figures 7d–7f). The air mass arriving in the morning above the ABL on 21 July is depleted in ozone as it was isolated from the ABL in the previous 48 h and had time to age. This back trajectory analysis indicates that air mass history is an important factor determining the magnitude, and potentially also the sign, of the effect of entrainment through ABL growth on surface ozone.

4.6. Morning Ozone Column Influencing Daytime Surface Concentrations

Here we investigate how ozone variability above the morning ABL (and therefore its differing potential for entrainment through ABL growth to pollute/dilute) influences ozone measured at the surface later in the day. Figure 8 shows how the morning (~8:00 LT) ozone averaged above the ABL up to 2.5 km AGL correlates with hourly averaged surface ozone concentrations 4 h later (at noon). An average from just above the ABL to 2.5 km was chosen since the highest observed ABL height was ~2.5 km. Linear fits through data from all sites are used because each individual site had too little data coverage to show a statistically significant slope. Linear fits for both observations and WRF-Chem, corresponding to the black lines in Figures 8a and 8b, respectively, are shown in Table 2 in bold.

Even though the data exhibits large scatter (small R^2) as well as differences between the sites, we find a small positive correlation and a slope statistically different from zero (p values around 0.08) on average for both the observations and for WRF-Chem. Table 2 compares the linear regression statistics between morning mean ozone concentrations above the ABL and hourly averaged surface ozone concentrations at different times later in the day between the observations and the model. This positive correlation could arise from the fact that conditions conductive to ozone production often persist for multiple days in a row, e.g., multiple successive hot, sunny days. The positive correlation may therefore reflect the memory of ozone from the previous day in the RL which is entrained the following day.

The influence of the early-morning above-ABL mean ozone on surface concentrations later in the day increases in both observations and model with increased slopes and correlation coefficients reaching a maximum 5 h after the morning (8:00 LT) soundings; corresponding to 13:00 LT. We interpret the 0.4 ppbv/ppbv slope for the noon-time observations as one additional ppbv of ozone above the ABL in the morning is associated with an increase of noon surface ozone by 0.4 ppbv on average. After 13:00 LT the correlation and slope between morning ozone concentrations aloft and surface ozone decreases. Differently, the modeled

Table 2. Slopes, Intercepts, Correlation Coefficients, and P Values for Linear Fits Through Observational and Model-Derived Data Showing the Relationship Between Morning Vertically Averaged (From z_i to 2500 m AGL) Column Concentrations Versus Surface Concentration at Times Between +1 and +12 h Later in the Day, Similar to That Shown in Figure 8 for Noon Time[a]

Hours After 8:00 A.M.	Observations (Slope (ppbv/ppbv); Intercept (ppbv); R^2, p)	WRF-Chem (Slope (ppbv/ppbv); Intercept (ppbv); R^2; p)
+ 1	(0.3 ± 0.3); (19.2 ± 20.0); 0.03; 0.31	(0.3 ± 0.2); (19.7 ± 10.0); 0.04; 0.20
+ 2	(0.2 ± 0.2); (29.4 ± 16.5); 0.02; 0.38	(0.3 ± 0.2); (24.0 ± 9.3); 0.04; 0.16
+ 3	(0.3 ± 0.2); (31.2 ± 14.1); 0.04; 0.21	(0.4 ± 0.2); (21.8 ± 8.0); 0.13; 0.01
+ 4	**(0.4 ± 0.2); (30.5 ± 13.1); 0.07; 0.09**	**(0.6 ± 0.2); (18.6 ± 8.1); 0.23; 0.001**
+ 5	(0.5 ± 0.3); (25.9 ± 17.2); 0.08; 0.08	(0.6 ± 0.2); (22.4 ± 9.0); 0.20; 0.002
+ 6	(0.4 ± 0.4); (32.8 ± 23.4); 0.03; 0.28	(0.6 ± 0.2); (25.4 ± 9.8); 0.18; 0.003
+ 7	(0.3 ± 0.4); (41.1 ± 26.2); 0.01; 0.50	(0.6 ± 0.2); (28.4 ± 10.7); 0.16; 0.01
+ 8	(0.1 ± 0.4); (54.9 ± 26.7); 0.00; 0.89	(0.6 ± 0.2); (28.3 ± 11.2); 0.14; 0.01
+ 9	(−0.2 ± 0.5); (71.5 ± 28.2); 0.00; 0.58	(0.6 ± 0.2); (24.8 ± 11.5); 0.13; 0.01
+ 10	(−0.2 ± 0.4); (66.7 ± 27.4); 0.00; 0.62	(0.5 ± 0.2); (26.8 ± 11.3); 0.09; 0.04
+ 11	(−0.1 ± 0.4); (56.1 ± 23.7); 0.00; 0.81	(0.5 ± 0.2); (22.6 ± 11.2); 0.09; 0.04
+ 12	(−0.1 ± 0.3); (47.9 ± 20.2); 0.00; 0.95	(0.5 ± 0.2); (18.3 ± 11.5); 0.08; 0.06

[a]Statistics for +4 h are presented here in bold.

correlations and slopes (Table 2) stay elevated, which points to a potential memory effect in the model that is not observed in nature or a cleansing effect that is observed in nature but not represented well in the model. A possible effect decreasing this correlation could be localized thunderstorms that are not reproduced well in the model. We observed such storms on ~50% of the flight days, usually in the afternoon. Another potential reason for this difference could be the fact that the vertical ozone above the boundary layer is more variable in the observations compared to the model (Figure 3). Similar analysis of influence of early-morning above-ABL correlation to maximum daily average 8 h (MDA8) surface O_3 concentrations reveal a much stronger slope of 0.6 ppbv/ppbv in the model versus a slope of 0.2 ppbv/ppbv in the observations.

4.7. Importance of Entrainment on the Total Ozone Budget

Finally, we investigate the relationship between the diurnal cycle of entrainment through ABL growth (discussed in section 4.4) and total ozone change over the course of the day. Total surface ozone changes (dO_3/dt) are calculated by differentiating hourly diurnal cycle surface ozone concentrations for each site. The diurnal cycle of dO_3/dt averaged over all six surface sites is shown in Figure 9a (black line); the observed maximum and minimum values are shown in gray. Similarly, the red line and red shaded area in Figure 9a show dO_3/dt from WRF-Chem at the grid points closest to the surface sites. The red and black dots with
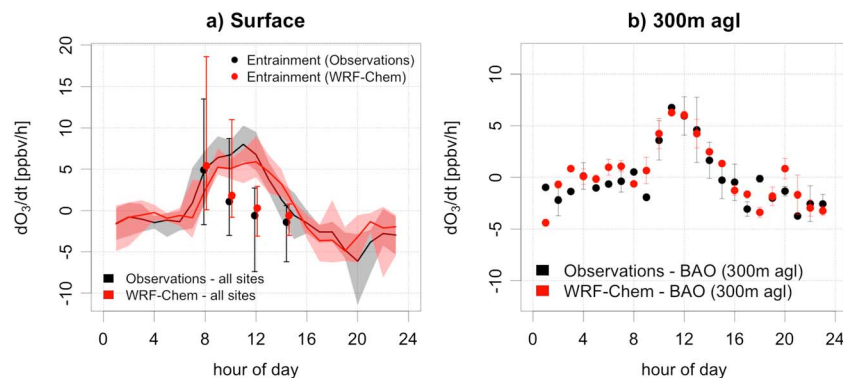

Figure 9. (a) The ozone change over time dO_3/dt is shown for all sites as an average (line) and the minimum and maximum in the shaded area observed at all six surface sites. In black are the observations and in red the model results. The black and red points with error bars are the mean, minimum, and maximum entrainment through ABL growth as shown in Figure 6 for observations and WRF-Chem, respectively. (b) The dO_3/dt measured (black) and modeled (red) at the BAO tower at 300 m AGL.

whiskers indicate the mean, minimum, and maximum entrainment through ABL growth values throughout the day for the observations and model results, respectively.

Before sunrise, total dO_3/dt is negative (-1 to -2 ppbv/h on average), indicating the importance of deposition and chemical loss due to reaction with NO occurring during the night. With sunrise, dO_3/dt turns positive and increases throughout the morning hours to reach 8 ppbv/h on average shortly before noon; this increase largely results from a combination of photochemical production, entrainment and advection and can additionally be masked by deposition and advection. After noon, dO_3/dt decreases to change sign again in the later afternoon around 15:00 LT. In the model, dO_3/dt starts to increase approximately one hour later in the day than found in the observations. The total dO_3/dt then increases steeply but only reaches 6 ppbv/h. The fall off of modeled dO_3/dt occurs again about one hour later than in the observations. At 300 m AGL, measured and modeled dO_3/dt (Figure 9b) are in good agreement throughout the day. Figures S5a–S5f show a similar analysis for surface-based observations/model data for each site separately. At three out of the six surface sites (Chatfield, Platteville, and Fort Collins) the modeled morning change in dO_3/dt from slightly negative values to strong ozone increase is 1 h later and overall weaker compared to the observations. At the other three sites (Golden, BAO, and Denver) the modeled dO_3/dt increase follows the observations well. The model captures the decrease of dO_3/dt after noon well at all sites but in Chatfield, where the model decreases 1 h later than the observations. At the BAO tower at 300 m AGL, dO_3/dt resembles the surface at the same location well with good agreement between observations and model.

The diurnal cycle of the total ozone change over time reflects the combination of advection, entrainment, deposition, chemical production, and loss (see equation (1)). All terms in equation (1) are expected to vary individually during a diurnal cycle, and their relative importance to the total ozone change evolves throughout the day. In urbanized regions, the leading term in the daytime ozone budget is typically the net photochemical production. This study allows us to compare the entrainment effect through ABL growth to the total ozone change, fully acknowledging that there is the potential for counteracting processes. Comparing the entrainment values through ABL growth from section 4.4 to the overall dO_3/dt discussed above suggests that entrainment through boundary layer growth is most important before 10:00 LT and with 5 ppbv/h which is of a similar order of magnitude to dO_3/dt at this time. An average value of 2 ppbv/h in the late morning indicates that entrainment through ABL growth remains influential between 10:00 LT and 12:00 LT (noon). After noon with values on the order of -1 ppbv/h, entrainment through ABL growth plays a diminishing role but can remain influential in slowing down the ozone concentration increase in the afternoon.

5. Conclusions

We use aircraft soundings of ozone collected during the July/August 2014 DISCOVER-AQ and FRAPPÉ campaigns in Colorado to calculate the diurnal evolution of entrainment through ABL growth and compare these to WRF-Chem modeled entrainment rates from ABL growth for the same region and time period. Similar to studies in the Southeastern U.S. [*Zhang and Rao*, 1999; *Kleinman et al.*, 1994], we also find in Colorado, that entrainment through ABL growth of ozone due to the growing boundary layer has the strongest effect on surface ozone concentrations in the morning when above ABL ozone is larger than ozone within the boundary layer. More specifically, we found that entrainment through ABL growth increases the surface ozone in the morning on average by 4.8 ppbv/h (range: -1.7 to 13.5 ppbv/h). The entrainment through ABL growth effect decreases in the late morning on average to 1.2 ppbv/h (-3.0 to 8.6 ppbv/h) and changes sign after noon to a slight dilution effect of, on average, -0.6 ppbv/h (-7.4 to 2.7 ppbv/h). This average dilution effect stays relatively constant at -1.4 ppbv/h (-6.2 to 0.6 ppbv/h) in the afternoon until the boundary layer stops growing around 16:00 LT. To the authors' knowledge, this is the first attempt to demonstrate the relationship between WRF-Chem predictions of the diurnal cycle of ozone entrainment through ABL growth and observations in the Colorado Front Range.

Our study presents a novel process-based strategy to make the comparison between observations and model results. Such process-based comparisons are important to determine uncertainties in the model especially for secondary pollutants such as ozone that have a variety of processes contributing to the overall diurnal cycle and magnitude at the surface. Predictions from a WRF-Chem simulation are interpolated in time and space to match the aircraft locations, and model results are analyzed similarly to the observations. To compare entrainment through ABL growth in the model to the observations, boundary layer growth, absolute

boundary layer height, ozone concentrations within and above the ABL, and ΔO_3 are compared. We find that the boundary layer grows nearly linearly with time between 8:00 and 15:00 LT with an average growth rate of 180 ± 20 m/h and 190 ± 20 m/h in the observations and the model, respectively. The time and areal average morning boundary layer depth in both the observations and model start at about 400 m at 8:00 LT (Figure 5). Due to the model's slightly higher growth rate, the simulated boundary layer depth at 16:00 LT reaches to about 2000 m on average, while the observed boundary layer depth averages approximately 1800 m.

Ozone concentrations at the surface are a few ppbv lower in the model than the observations throughout the day. In the mixed layer and free troposphere sampled by the aircraft, morning absolute ozone concentrations both below and above the top of the boundary layer are 10–15 ppbv lower in the model than in the measurements. Ozone in the boundary layer increases through the morning at an average rate of about 4–5 ppbv/h in both the observations and the model. Ozone above the boundary layer increases slightly faster in the model (at a rate of 1.5–3 ppbv/h) compared to that found in the observations (where the rate is 1–1.5 ppbv/h). This leads to ozone gradients across the top of the boundary layer (ΔO_3) in the morning that are well reproduced by the model and higher modeled ΔO_3 than observed for the rest of the day. Throughout the day, entrainment rates through ABL growth in WRF-Chem are 0.6–0.8 ppbv/h higher than the observed rates, this is due to a combination of differences in ABL height, growth and ΔO_3.

The observations show large day-to-day variability of ozone concentrations above the ABL. This variability is attributed to differing air mass origins using HYSPLIT back trajectory analysis. Analyzing the air mass origin of the highest and lowest ozone concentrations observed above the boundary layer indicates that air masses transported over the continental U.S. at high altitudes resulted in a morning concentration above ABL of 55 ppbv ozone versus recirculation of air masses at lower altitudes in Colorado and neighboring states resulted in a morning concentration above ABL of 70–90 ppbv. Morning (8 am) ozone vertical mean concentration from the boundary layer top up to 2.5 km AGL were found to influence surface concentrations most strongly at 13:00 LT; a feature which is also well captured by the model. Later in the day this influence vanishes in the observations but persists in the model. Possible reasons could be underrepresentation of local thunderstorms in the model or too little vertical variability in ozone concentrations above the boundary layer in the model.

The total ozone budget at the surface and its diurnal cycle are influenced by a variety of physical processes, all of which are expected to contribute differently to the total budget throughout a diurnal cycle. A total dO_3/dt of −1 to −5 ppbv/h during nighttime is followed by a steep linear increase in the early morning reaching up to 8 ppbv/h at noon and decreases similarly fast to reach negative values in the late afternoon again. The model underestimates the peak of dO_3/dt at the surface, and the timing for the increase and the decrease are both delayed by 1 h compared to the observations. To fully understand and study the total O_3 budget with all its individual terms, it is important to add surface flux measurements and advection measurements in future studies.

References

AirNow, A look back: Ozone in (2015), [Available at https://gispub.epa.gov/OAR_OAQPS/SeasonReview2015/index.html?appid=bc823213d0ae41ab9445efbf48ad6b94.]

Anderson, D. C., et al. (2014), Measured and modeled CO and NO_y in DISCOVER-AQ: An evaluation of emissions and chemistry over the eastern US, *Atmos. Environ.*, 96, 78–87, doi:10.1016/j.atmosenv.2014.07.004.

Angevine, W. M. (1999), Entrainment results including advection and case studies from the flatland boundary layer experiments, *J. Geophys. Res.*, 104, 30,947–30,963, doi:10.1029/1999JD900930.

Baier, B., et al. (2017), Higher measured than modeled ozone production at increased NO_x levels in the Colorado Front Range, *Atmos. Chem. Phys. Discuss.*, doi:10.5194/acp-2016-1089.

Baier, B. C., W. H. Brune, B. L. Lefer, D. O. Miller, and D. K. Martins (2015), Direct ozone production rate measurements and their use in assessing ozone source and receptor regions for Houston in 2013, *Atmos. Environ.*, 114, 83–91, doi:10.1016/j.atmosenv.2015.05.033.

Cazorla, M., W. H. Brune, X. Ren, and B. Lefer (2012), Direct measurement of ozone production rates in Houston in 2009 and comparison with two estimation methods, *Atmos. Chem. Phys.*, 12, 1203–1212, doi:10.5194/acp-12-1203-2012.

Chameides, W. L., et al. (1992), Ozone precursor relationships in the ambient atmosphere, *J. Geophys. Res.*, 97, 6037–6055, doi:10.1029/91JD03014.

Chen, F., and J. Dudhia (2001), Coupling an advanced land-surface/hydrology model with the Penn State/NCAR MM5 modeling system. Part I: Model description and implementation, *Mon. Weather Rev.*, 129, 569–585, doi:10.1175/1520-0493(2001)129<0569:CAALSH>2.0.CO;2.

Chuang, M.-T., Y. Zhang, and D.-W. Kang (2011), Application of WRF/Chem-MADRID for real-time air quality forecasting over the southeastern United States, *Atmos. Environ.*, 45(34), 6241–6250, doi:10.1016/j.atmosenv.2011.06.071.

Conley, S. A., et al. (2011), A complete dynamical ozone budget measured in the tropical marine boundary layer during PASE, *J. Atmos. Chem.*, 68, 55, doi:10.1007/s10874-011-9195-0.

Denmead, O. T., M. R. Raupach, F. X. Dunin, H. A. Cleugh, and T. Leuning (1996), Boundary layer budgets for regional estimates of scalar fluxes, *Global Change Biol.*, *2*(3), 255–264, doi:10.1111/j.1365-2486.1996.tb00077.x.

Dentener, F., Keating, T., and H. Akimoto (Eds.) (2011), *Hemispheric Transport of Air Pollution 2010: Part A: Ozone and Particulate Matter*, *Air Pollut. Stud.*, vol. 17, pp. 1–24, United Nations, New York and Geneva.

DISCOVER-AQ Science Team (2016), NASA Atmospheric Science Data Center (ASDC), Hampton, Va, Accessed October 2016 at doi: 10.5067/Aircraft/DISCOVER-AQ/Aerosol-TraceGas.

Environmental Protection Agency (2016), Determinations of attainment by the attainment date, extensions of the attainment date, and reclassification of several areas for the 2008 ozone National Ambient Air Quality Standards, Federal Register, 81,87, 26697–28722, May 4, 2016.

Fann, N., A. D. Lamson, S. C. Anenberg, K. Wesson, D. Risley, and B. J. Hubbell (2012), Estimating the National Public Health burden associated with exposure to ambient PM2.5 and ozone, *Risk Anal.*, *32*, 81–95, doi:10.1111/j.1539-6924.2011.01630.x.

Fast, J. D., W. I. Gustafson Jr., R. C. Easter, R. A. Zaveri, J. C. Barnard, E. G. Chapman, and G. A. Grell (2006), Evolution of ozone, particulates, and aerosol direct forcing in an urban area using a new fully-coupled meteorology, chemistry, and aerosol model, *J. Geophys. Res.*, *111*, D21305, doi:10.1029/2005JD006721.

Fedorovich, E., R. Conzemius, and D. Mironv (2004), Convective entrainment into a shear-free, linearly stratified atmosphere: Bulk models reevaluated through large eddy simulations, *J. Atmos. Sci.*, *61*, 281–295, doi:10.1175/1520-0469(2004)061<0281:CEIASL>2.0.CO;2.

Grell, G. A. (1993), Prognostic evaluation of assumptions used by cumulus parameterizations, *Mon. Weather Rev.*, *121*, 764–787, doi:10.1175/1520-0493(1993)121<0764:PEOAUB>2.0.CO;2.

Grell, G. A., and D. Devenyi (2002), A generalized approach to parameterizing convection combining ensemble and data assimilation techniques, *Geophys. Res. Lett.*, *29*(14), 1693, doi:10.1029/2002GL015311.

Grell, G. A., S. E. Peckham, R. Schmitz, S. A. McKeen, G. Frost, W. C. Skamarock, and B. Eder (2005), Fully coupled "online" chemistry within the WRF model, *Atmos. Environ.*, *39*(37), 6957–6975, doi:10.1016/j.atmosenv.2005.04.027.

Guenther, A., T. Karl, P. Harley, C. Wiedinmyer, P. I. Palmer, and C. Geron (2006), Estimates of global terrestrial isoprene emissions using MEGAN (model of emissions of gases and Aerosols from nature), *Atmos. Chem. Phys.*, *6*, 3181–3210, doi:10.5194/acp-6-3181-2006.

Hong, S. Y. (2010), A new stable boundary-layer mixing scheme and its impact on the simulated east Asian summer monsoon, *Q. J. R. Meteorol. Soc.*, *136*(651), 1481–1496, doi:10.1002/Qj.665.

Hong, S. Y., Y. Noh, and J. Dudhia (2006), A new vertical diffusion package with an explicit treatment of entrainment processes, *Mon. Weather Rev.*, *134*(9), 2318–2341, doi:10.1175/Mwr3199.1.

Hu, X.-M., J. W. Nielsen-Gammon, and F. Zhang (2010), Evaluation of three planetary boundary layer schemes in the WRF model, *J. Appl. Meteorol. Climatol.*, *49*(9), 1831–1844, doi:10.1175/2010jamc2432.1.

Iacono, M. J., J. S. Delamere, E. J. Mlawer, M. W. Shephard, S. A. Clough, and W. D. Collins (2008), Radiative forcing by long-lived greenhouse gases: Calculations with the AER radiative transfer models, *J. Geophys. Res.*, *113*, D13103, doi:10.1029/2008JD009944.

Im, U., et al. (2015), Evaluation of operational on-line-coupled regional air quality models over Europe and North America in the context of AQMEII phase 2. Part I: Ozone, *Atmos. Environ.*, *115*, 404–420, doi:10.1016/j.atmosenv.2014.09.042.

Jacob, D. J., J. A. Logan, and P. P. Murti (1999), Effect of rising Asian emissions on surface ozone in the United States, *Geophys. Res. Lett.*, *26*, 2175–2178, doi:10.1029/1999GL900450.

Jaffe, D. (2011), Relationship between surface and free tropospheric ozone in the western U.S., *Environ. Sci. Technol.*, *45*(2), 432–438, doi:10.1021/es1028102.

Janjic, Z. I. (1996), The surface layer in the NCEP Eta model, in *Proceedings of the 11th Conference on Numerical Weather Prediction*, Am. Meteorol. Soc., pp. 354–355, Norfolk, Va.

Janjic, Z. I. (2002), Nonsingular implementation of the Mellor–Yamada level 2.5 scheme in the NCEP Meso model, NCEP Office Note, 437, 61.

Kleinman, L. I. (2005), The dependence of tropospheric ozone production rate on ozone precursors, *Atmos. Environ.*, *39*(3), 575–586, doi:10.1016/j.atmosenv.2004.08.047.

Kleinman, L. I., et al. (1994), Ozone formation at a rural site in the southeastern United States, *J. Geophys. Res.*, *99*, 3469–6482, doi:10.1029/93JD02991.

Knote, C., et al. (2014), Simulation of semi-explicit mechanisms of SOA formation from glyoxal in aerosol in a 3-D model, *Atmos. Chem. Phys.*, *14*, 6213–6239, doi:10.5194/acp-14-6213-2014.

Lenschow, D. H., R. Pearson Jr., and B. B. Stankov (1981), Estimating the ozone budget in the boundary layer by use of aircraft measurements of ozone eddy flux and mean concentration, *J. Geophys. Res.*, *86*, 7291–7297, doi:10.1029/JC086iC08p07291.

Liu, S. C., et al. (1992), A study of the photochemistry and ozone budget during the Mauna Loa Observatory photochemistry experiment, *J. Geophys. Res.*, *97*, 10,463–10,471, doi:10.1029/91JD02298.

Logan, J. A., M. J. Prather, S. C. Wofsy, and M. B. McElroy (1981), Tropospheric chemistry: A global perspective, *J. Geophys. Res.*, *86*, 7210–7254, doi:10.1029/JC086iC08p07210.

Mar, K. A., N. Ojha, A. Pozzer, and T. M. Butler (2016), Ozone air quality simulations with WRF-Chem (v3.5.1) over Europe: Model evaluation and chemical mechanism comparison, *Geosci. Model Dev.*, *9*, 3699–3728, doi:10.5194/gmd-9-3699-2016.

McClure-Begley, A., I. Petropavlovskikh, and S. Oltmans (2014), NOAA global monitoring surface ozone network, National Oceanic and Atmospheric Administration, Earth Systems Research Laboratory Global Monitoring Division. Boulder, Colo., doi:10.7289/V57P8WBF.

Monin, A. S., and A. M. Obukhov (1954), Basic laws of turbulent mixing in the surface layer of the atmosphere, *Contrib. Geophys. Inst. Slovak Acad. Sci.*, *24*(151), 163–187.

Münkel, C. (2007), Mixing height determination with lidar ceilometers—Results from Helsinki testbed, *Meteorol. Z.*, *16*, 451–459.

Pagowski, M., G. A. Grell, S. A. McKeen, S. E. Peckham, and D. Devenyi (2010), Three-dimensional variational data assimilation of ozone and fine particulate matter observations: Some results using the weather research and forecasting—Chemistry model and grid-point statistical interpolation, *Q. J. R. Meteorol. Soc.*, *136*, 2013–2024, doi:10.1002/qj.700.

Parrish, D. D., K. C. Aikin, S. J. Oltmans, B. J. Johnson, M. Ives, and C. Sweeny (2010), Impact of transported background ozone inflow on summertime air quality in a California ozone exceedance area, *Atmos. Chem. Phys.*, *10*, 10,093–10,109, doi:10.5194/acp-10-10093-2010.

Pfister, G. G., S. Walters, L. K. Emmons, D. P. Edwards, and J. Avise (2013), Quantifying the contribution of inflow on surface ozone over California during summer 2008, *J. Geophys. Res. Atmos.*, *118*, 12,282–12,299, doi:10.1002/2013JD020336.

Ridley, B. A., and F. E. Grahek (1990), A small, low flow, high-sensitivity reaction vessel for NO chemiluminescence detectors, *J. Atmos. Oceanic Technol.*, *7*, 307–311, doi:10.1175/1520-0426(1990)007<0307:ASLFHS>2.0.CO;2.

Ridley, B. A., F. E. Grahek, and J. G. Walega (1992), A small, high-sensitivity, medium-response ozone detector suitable for measurements from light aircraft, *J. Atmos. Oceanic Technol.*, *9*, 142–148, doi:10.1175/1520-0426(1992)009<0142:ASHSMR>2.0.CO;2.

Schäfer, K., P. Wagner, S. Emeis, C. Jahn, C. Münkel, and P. Suppa (2012), Mixing layer height and air pollution levels in urban area, Proc. SPIE 8534, Remote Sensing of Clouds and the Atmosphere XVII; and Lidar Technologies, Techniques, and Measurements for Atmospheric Remote Sensing VIII; doi:10.1117/12.974328.

Stein, A. F., R. R. Draxler, G. D. Rolph, B. J. B. Stunder, M. D. Cohen, and F. Ngan (2015), NOAA's HYSPLIT atmospheric transport and dispersion modeling system, *Bull. Am. Meteorol. Soc.*, *96*, 2059–2077, doi:10.1175/BAMS-D-14-00110.1.

Stevenson, D. S., et al. (2006), Multimodel ensemble simulations of present-day and near-future tropospheric ozone, *J. Geophys. Res.*, *111*, D08301, doi:10.1029/2005JD006338.

Spinhirne, J. D. (1993), Micro pulse lidar, *IEEE Trans. Geosci. Remote Sens.*, *31*, 48–55.

Stull, R. B. (1988), *An Introduction to Boundary Layer Meteorology*, pp. 441–497, Kluwer Acad., Dordrecht, Netherlands.

Sullivan, J. T., T. J. McGee, A. M. Thompson, R. B. Pierce, G. K. Sumnicht, L. W. Twigg, E. Eloranta, and R. M. Ho (2015), Characterizing the lifetime and occurrence of stratospheric-tropospheric exchange events in the rocky mountain region using high-resolution ozone measurements, *J. Geophys. Res. Atmos.*, *120*, 12,410–12,424, doi:10.1002/2015JD023877.

Rolph, G. D. (2016), Real-time Environmental Applications and Display sYstem (READY), NOAA Air Resour. Lab., College Park, Md. [Available at http://www.ready.noaa.gov.]

Tennekes, H. (1973), A model for the dynamics of the inversion above a convective boundary layer, *J. Atmos. Sci.*, *30*, 558–567, doi:10.1175/1520-0469(1973)030<0558:AMFTDO>2.0.CO;2.

Thompson, G., P. R. Field, R. M. Rasmussen, and W. D. Hall (2008), Explicit forecasts of winter precipitation using an improved bulk microphysics scheme. Part II: Implementation of a new snow parameterization, *Mon. Weather Rev.*, *136*, 5095–5115, doi:10.1175/2008MWR2387.1.

Trousdell, J. F., S. A. Conley, A. Post, and I. C. Faloona (2016), Observing entrainment mixing, photochemical ozone production, and regional methane emissions by aircraft using a simple mixed-layer model, *Atmos. Chem. Phys.*, *16*, 15,433–15,450, doi:10.5194/acp-16-15433-2016.

van Dingenen, R., F. J. Dentener, F. Raes, M. C. Krol, L. Emberson, and J. Cofala (2009), The global impact of ozone on agricultural crop yields under current and future air quality legislation, *Atmos. Environ.*, *43*, 604–618, doi:10.1016/j.atmosenv.2008.10.033.

Wesely, M. L., and B. B. Hicks (2000), A review of the current status of knowledge on dry deposition, *Atmos. Environ.*, *34*(12–14), 2261–2282, doi:10.1016/S1352-2310(99)00467-7.

Wiedinmyer, C., S. K. Akagi, R. J. Yokelson, L. K. Emmons, J. A. Al-Saadi, J. J. Orlando, and A. J. Soja (2011), The Fire INventory from NCAR (FINN): A high resolution global model to estimate the emissions from open burning, *Geosci. Model Dev.*, *4*, 625–641, doi:10.5194/gmd-4-625-2011.

World Health Organization (2013), *Review of Evidence on Health Aspects of Air Pollution—REVIHAAP Project: Final Technical Report*, pp. 47–66, WHO Regional Office for Europe, Copenhagen.

Zhang, J., and S. T. Rao (1999), The role of vertical mixing in the temporal evolution of ground-level ozone concentrations, *J. Appl. Meteorol.*, *38*(12), 1674–1691, doi:10.1175/1520-0450(1999)038<1674:TROVMI>2.0.CO;2.

Zhang, Y., et al. (2016), Large vertical gradient of reactive nitrogen oxides in the boundary layer: Modeling analysis of DISCOVER-AQ 2011 observations, *J. Geophys. Res. Atmos.*, *121*, 1922–1934, doi:10.1002/2015JD024203.